REDISCUSSION OF ECLIPSING BINARIES. PAPER 16: THE δ SCUTI / γ DORADUS HYBRID PULSATOR GK DRACONIS

By John Southworth

Astrophysics Group, Keele University

GK Dra is a detached eclipsing binary system containing two early-F stars, one evolved, in an orbit with a period of 9·974 d and a small eccentricity. Its eclipsing nature was discovered using *Hipparcos* data, and pulsations were found in follow-up ground-based data. Extensive observations have been obtained using the *Transiting Exoplanet Survey Satellite* (*TESS*), and we use these and published spectroscopy to perform a detailed reanalysis of the system. We determine masses of 1·421±0·012 and 1·775±0·028 $M_{\odot}$, and radii of 1·634±0·011 and 2·859±0·028 $R_{\odot}$. The secondary component is more massive, larger, and slightly cooler than its companion; the eclipses are total. The properties of the system can be matched by theoretical predictions for an age of 1·4 Gyr and a slightly sub-solar metallicity. We measure 15 significant pulsation frequencies in the *TESS* light-curve, of which three are in the frequency domain of γ Doradus pulsations and the remaining 12 are δ Scuti pulsations; the system is thus a hybrid pulsator. The strongest pulsation can be definitively assigned to the secondary star as it has been detected in radial velocities of that object. *TESS* will observe GK Dra again for ten consecutive sectors in the near future.

Introduction

Eclipsing binary star systems contain the only stars for which a direct measurement of their most basic properties (mass and radius) is obtainable. Detached eclipsing binaries (dEBs) are particularly useful because their components have evolved as single stars so can be compared to the predictions of theoretical models of stellar evolution, both to check how well the models perform and to guide their improvement[1–3].

Another approach to constraining the theoretical descriptions of stars is *via* asteroseismology[4], which uses the measurement of stellar oscillation frequencies to constrain properties such as their densities, ages, and rotational profiles[5–8].

A significant fraction of stars are known to show the signatures of both eclipses and pulsations in their light-curves. Many of these identifications are a result of the widespread availability of high-quality light-curves from space-based telescopes[9]. The most common class of pulsations seen in dEBs is the δ Scuti type[10–12], which are short-period pulsations (0·015 to 0·33 d[13,14]) with pressure as the restoring force. A smaller number show γ Doradus pulsations[15,16], which have longer periods (0·3 d to 4 d[14,17]) and gravity as their restoring force. The δ Scuti and γ Dor phenomena can occur simultaneously in late-A and early-F stars, examples of which are labelled as hybrid pulsators[14,18].

In this work we present an analysis of GK Draconis based on published spectroscopy and new space-based photometry. GK Dra is a dEB known to display δ Scuti pulsations. We find that it also shows γ Dor pulsations. For further discussion on the motivation of this series of papers see ref. 19.

GK Draconis

GK Dra (Table I) is one of the 343 eclipsing binaries discovered using data from the *Hipparcos* satellite[25] and named by Kazarovets *et al.*[26]. Dallaporta *et al.*[27] presented the first ground-based photometry, finding an orbital period of $P = 9{\cdot}9742$ d, a modest orbital eccentricity, and pulsations in the secondary component consistent with the δ Scuti type. The system has since been included in catalogues of binary systems containing δ Scuti components[28,29].

Griffin & Boffin[30] (hereafter GB03) published the first radial-velocity (RV) study of GK Dra and V1094 Tau (the latter since analysed in detail by Maxted *et al.*[31]). For GK Dra they obtained 50 RVs of each star. A large scatter in the RVs of the more massive component was found and attributed to the effects of pulsations. A variation of 0·1178-d period was included in the fit to the spectroscopic orbit of the star to account for the pulsation signature. This variation was treated as a Keplerian orbit for convenience, and the fitted eccentricity and velocity amplitudes were $e = 0{\cdot}26 \pm 0{\cdot}06$ and $2{\cdot}62 \pm 0{\cdot}17$ km s^{-1}, respectively. The RVs for the less massive star were also found to show an excess scatter indicative of possible pulsations. GB03 found the spectral types of both components to be significantly earlier than the G0 given in the *Henry Draper Catalogue*[21] based on the $B-V$ colour index and the presence of pulsations in at least one of the stars, preferring F2 III–IV for the more massive star.

Zwitter *et al.*[32] (hereafter ZW03) presented the only full analysis of GK Dra published so far. They based their results on data from the *Hipparcos* satellite plus a set of 35 échelle spectra covering 848–874 nm, specifically chosen to simulate the type of data expected from the *Gaia* mission[33]. The masses and radii thus determined were $M_{\rm A} = 1{\cdot}46 \pm 0{\cdot}07\ M_{\odot}$, $M_{\rm B} = 1{\cdot}81 \pm 0{\cdot}11\ M_{\odot}$, $R_{\rm A} = 2{\cdot}43 \pm 0{\cdot}04\ R_{\odot}$ and $R_{\rm B} = 2{\cdot}83 \pm 0{\cdot}05\ R_{\odot}$. These numbers indicate that both components are significantly evolved. The RVs from ZW03 are not of the same quality as those from GB03, and the *Hipparcos* photometry is greatly inferior to that now available from *TESS*, so a reanalysis of GK Dra is warranted.

Table I

Basic information on GK Draconis

Property	*Value*	*Reference*
Right ascension (J2000)	$16^{\rm h}45^{\rm m}41^{\rm s}{\cdot}19$	20
Declination (J2000)	$+68°15'30''.9$	20
Henry Draper designation	HD 152088	21
Gaia DR3 designation	1648575062872337792	20
Gaia DR3 parallax	$3{\cdot}2954 \pm 0{\cdot}0133$ mas	20
TESS Input Catalog designation	TIC 230128667	22
B magnitude	$9{\cdot}12 \pm 0{\cdot}02$	23
V magnitude	$8{\cdot}77 \pm 0{\cdot}01$	23
J magnitude	$8{\cdot}001 \pm 0{\cdot}023$	24
H magnitude	$7{\cdot}886 \pm 0{\cdot}021$	24
$K_{\rm s}$ magnitude	$7{\cdot}864 \pm 0{\cdot}024$	24
Spectral type	F1 V + F2 IV	This work

Photometric observations

GK Dra has been observed extensively by the NASA *Transiting Exoplanet Survey Satellite*[34] (*TESS*) as it lies in the northern continuous viewing zone of that telescope. Data from sectors 14 to 26 (2019/07/18 to 2020/07/04) were obtained at a cadence of 1800 s, although those from sectors 15 and 16 were not available from the archive at the time of writing. Sectors 40 and 41 (2021/06/08 to 2021/08/20), and 47 to 55 (2021/12/30 to 2022/09/01) yield data at a cadence of 600 s. Finally, in sectors 56 to 60 (2022/09/01 to 2023/01/18) GK Dra was observed at a 200-s cadence.

The data from all the sectors mentioned above were downloaded from the NASA Mikulski Archive for Space Telescopes (MAST*) using the LIGHTKURVE package[35]. The 'hard' flag was used to reject data labelled as of lower quality. We used the simple aperture photometry (SAP) data[36] for consistency with previous papers in this series. The data were converted to differential magnitude and the median magnitude of each sector was subtracted for convenience.

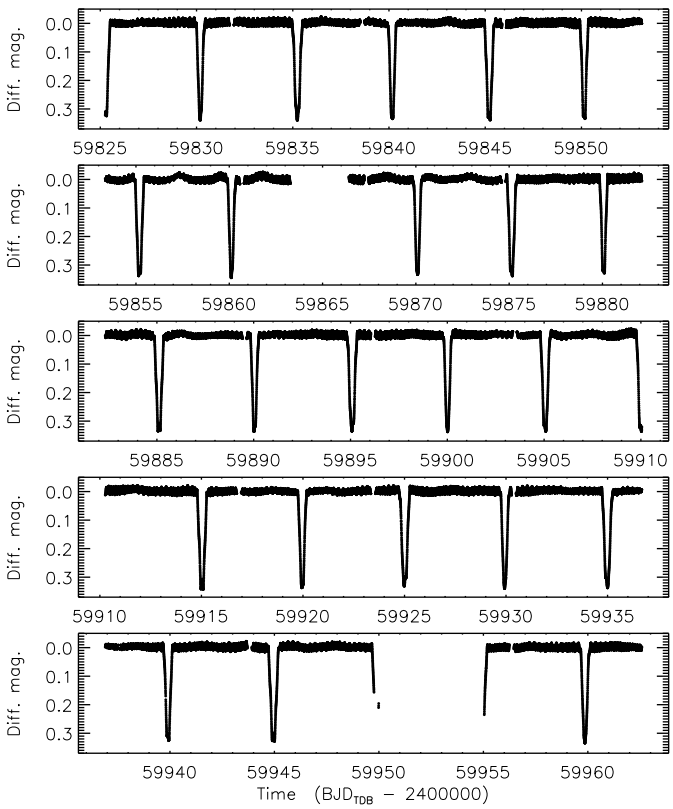

FIG. 1

TESS short-cadence SAP photometry of GK Dra. The flux measurements have been converted to magnitude units then rectified to zero magnitude by subtraction of the median.

*https://mast.stsci.edu/portal/Mashup/Clients/Mast/Portal.html

Our results below are primarily based on the 600-s-cadence data as these cover many eclipses whilst avoiding problems with undersampling the light variations of the system. We used the 200-s-cadence data for the pulsation analysis due to its higher frequency resolution. The 200-s data are shown in Fig. 1, where eclipses and pulsations can both be seen. The 600-s data look similar but of course have a lower sampling rate.

We queried the *Gaia* DR3 database* for objects within 2 arcmin of GK Dra. Only nine were found, and all are fainter by at least 6·3 mag in the *G* band, so contamination from these objects is negligible.

Light-curve analysis

Due to the number and variety of *TESS* data available for GK Dra, we investigated two choices with which to develop a model of the system. The first choice was to use only the 200-s-cadence data (sectors 56–60) as they have the highest available sampling rate; this was successful but led to a lower precision than desired in the final results. We therefore also modelled the 600-s-cadence data from sectors 47–55, augmented by the data from sectors 56–60 reduced to 600-s cadence for consistency.

In both cases we extracted the data within 0·6 d of an eclipse from the full datasets, in order to speed up the computation times in our analysis. The data around each eclipse were individually fitted with a straight line to normalize them to zero differential magnitude, and eclipses which were not fully covered by the data were rejected. This left us with 9730 data points (out of 53 296) for the 200-s light-curve and 10 497 data points (out of 47 378) for the 600-s light-curve. In both cases we ignored the error bars supplied with the *TESS* data as they do not account for the pulsations.

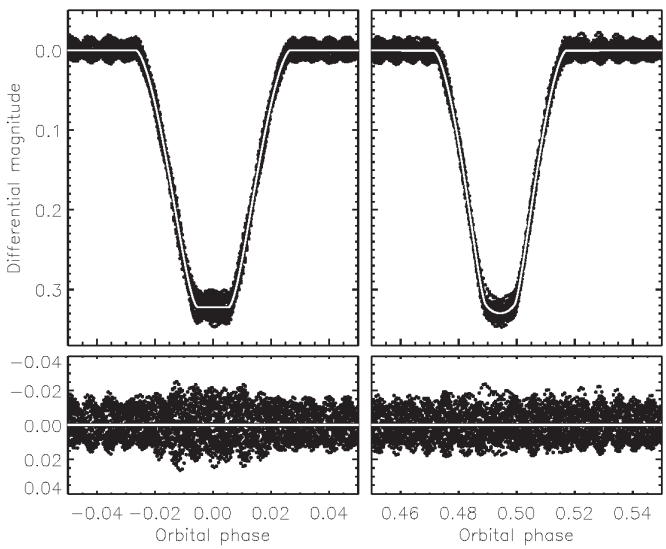

Fig. 2

The 600-s-cadence *TESS* light-curves of GK Dra (filled circles) and its best fit from jktebop (white-on-black line) *versus* orbital phase. The primary eclipse is shown on the left and the secondary eclipse on the right. The residuals are shown on an enlarged scale in the lower panel.

*https://vizier.cds.unistra.fr/viz-bin/VizieR-3?-source=I/355/gaiadr3

TABLE II

Parameters of GK Dra measured from the TESS light-curves using the JKTEBOP code. The uncertainties are 1σ and were determined using residual-permutation simulations. We give the results for both the 200-s- and 600-s-cadence data. We adopted the results for the 600-s-cadence data but with error bars double those reported in this table.

Parameter	*Value (200s)*	*Value (600s)*
Fitted parameters:		
Primary eclipse time (BJD_{TDB})	2459905·05884 ± 0·00020	2459905·05884 ± 0·00024
Orbital period (d)	9·974128 ± 0·000053	9·974128 ± 0·000012
Orbital inclination (°)	88·27 ± 0·11	88·467 ± 0·062
Sum of the fractional radii	0·15687 ± 0·00065	0·15641 ± 0·00042
Ratio of the radii	1·791 ± 0·023	1·750 ± 0·010
Central-surface-brightness ratio	1·027 ± 0·048	0·938 ± 0·015
LD coefficient c	0·670 ± 0·086	0·584 ± 0·048
LD coefficient α	0·448 (fixed)	0·448 (fixed)
$e \cos \omega$	−0·008985 ± 0·000041	−0·009000 ± 0·000036
$e \sin \omega$	−0·07811 ± 0·0021	−0·07998 ± 0·0017
Derived parameters:		
Fractional radius of star A	0·05620 ± 0·00028	0·05689 ± 0·00014
Fractional radius of star B	0·10067 ± 0·00087	0·09953 ± 0·00044
Light ratio ℓ_B/ℓ_A	3·30 ± 0·24	2·87 ± 0·073
Orbital eccentricity	0·0786 ± 0·0022	0·0805 ± 0·0017
Argument of periastron (°)	263·44 ± 0·18	263·58 ± 0·14

We modelled the light-curves using version 43 of the JKTEBOP* code[37,38]. The fitted parameters included the sum ($r_A + r_B$) and ratio ($k = r_B/r_A$) of the fractional radii of the stars (r_A and r_B), the central surface-brightness ratio ($\mathcal{J}$), orbital inclination (i), orbital period (P), and a reference time of primary minimum (T_o). The orbital eccentricity (e) and argument of periastron (ω) were included as $e \cos \omega$ and $e \sin \omega$ to avoid their mutual correlation. Limb darkening was included in our model using the power-2 law[39,40]: we fitted for the c coefficients and fixed the α coefficients to a theoretically-predicted value[41,42]. Third light was fixed at zero as attempts to fit it yielded a small negative value. The lower sampling rate of the 600-s-cadence data might bias the measurements of the fitted parameters[43]. We checked this by running fits where the model was numerically integrated to match the data[43], finding a negligible change in the parameter values. We conclude that the sampling rate does not have a significant effect on the results given in Table II.

The depths of the primary and secondary eclipses are visually inseparable due to the similar T_{eff} values of the stars and the pulsational variability. However, our fits reliably converged to a situation in which the larger and more massive star is slightly cooler, in agreement with the results of ZW03. We therefore define star A to be the hotter but less massive star — it is the one eclipsed at the primary (deeper) eclipse. Star B is thus eclipsed at the secondary eclipse (which occurs at phase 0·4943) and is significantly larger and brighter than star A. The *TESS* data reveal that the eclipses are total†.

For the record, we were able to fit the light-curve quite well with the inverse of the ratio of the radii ($k = 0{\cdot}56$ in this case). This local-minimum solution could

*http://www.astro.keele.ac.uk/jkt/codes/jktebop.html

†To be precise, the primary eclipse is total and the secondary eclipse is annular.

be rejected because the limb darkening caused curvature in the wrong eclipse (secondary *versus* primary) and thus did not match the data.

The uncertainties in the fitted parameters were determined using residual-permutation simulations[44], treating the pulsational variation as red noise. Similar uncertainties were found by modelling the sectors of data individually[45]. See our recent paper on V1765 Cyg[46] for example plots from a similar residual-permutation analysis. The agreement between the results for the 200-s- and 600-s-cadence data is not as good as hoped, with differences between parameters of typically one to two times the size of the uncertainties. As we found above that the lower cadence of the 600-s data was not important, we adopted the results from these data but with the error bars doubled.

Pulsation analysis

The *TESS* light-curve of GK Dra shows clear evidence for pulsations. The strongest frequency (f_8) was detected in the RVs of star B by GB03 so can be unambiguously attributed to that star. We fitted the 200-s-cadence data with JKTEBOP and subtracted the best-fitting model of the light-curve. The residuals of the fit were passed to version 1.2.0 of the PERIOD04 code[47] and a frequency spectrum was calculated from 0 to the Nyquist frequency of 216 d^{-1}. No significant periodicity was found beyond 30 d^{-1} (Fig. 3).

We measured a total of 15 significant frequencies in the frequency spectrum, adopting as our significance criterion a signal-to-noise ratio (S/N) greater than 4 (refs. 48, 49). We then fitted sinusoids simultaneously to all of them to obtain their amplitudes and phases. The uncertainties of the fitted parameters were calculated using both a standard least-square fit and Monte Carlo simulations, the latter being larger.

The results are given in Table III. We find three low frequencies (f_1 to f_3) near 0·46 d^{-1} which are likely of the γ Doradus type. The strongest pulsation (f_8) has a frequency of 8·49070 ± 0·00004 d^{-1} (period 0·1177759 ± 0·0000006 d) and amplitude of 10·6 mmag; this is in wonderful agreement with the periodicity of 0·1177753 ± 0·0000005 d found in the RVs of star B by GB03. There are groups

TABLE III

Significant pulsation frequencies found in the TESS 200-s-cadence light-curve of GK Dra after subtraction of the effects of binarity.

Label	*Frequency* (d^{-1})	*Amplitude* (*mmag*)	*Phase*
f_1	0·44029 ± 0·00003	2·253 ± 0·024	0·436 ± 0·002
f_2	0·46049 ± 0·00007	1·297 ± 0·026	0·657 ± 0·002
f_3	0·48624 ± 0·00007	0·964 ± 0·230	0·912 ± 0·073
f_4	3·83445 ± 0·00020	0·366 ± 0·018	0·119 ± 0·007
f_5	4·30136 ± 0·00017	0·398 ± 0·017	0·646 ± 0·007
f_6	4·66593 ± 0·00010	0·770 ± 0·019	0·330 ± 0·004
f_7	4·84289 ± 0·00006	1·226 ± 0·020	0·563 ± 0·003
f_8	8·49070 ± 0·00004	10·574 ± 0·027	0·135 ± 0·001
f_9	8·55349 ± 0·00003	2·191 ± 0·106	0·578 ± 0·002
f_{10}	16·73503 ± 0·00032	0·255 ± 0·018	0·242 ± 0·011
f_{11}	16·98151 ± 0·00010	0·627 ± 0·289	0·283 ± 0·004
f_{12}	17·00896 ± 0·00020	0·322 ± 0·039	0·788 ± 0·008
f_{13}	25·22548 ± 0·00155	0·041 ± 0·016	0·799 ± 0·061
f_{14}	25·47241 ± 0·00158	0·040 ± 0·019	0·781 ± 0·063
f_{15}	25·49961 ± 0·00150	0·042 ± 0·020	0·137 ± 0·069

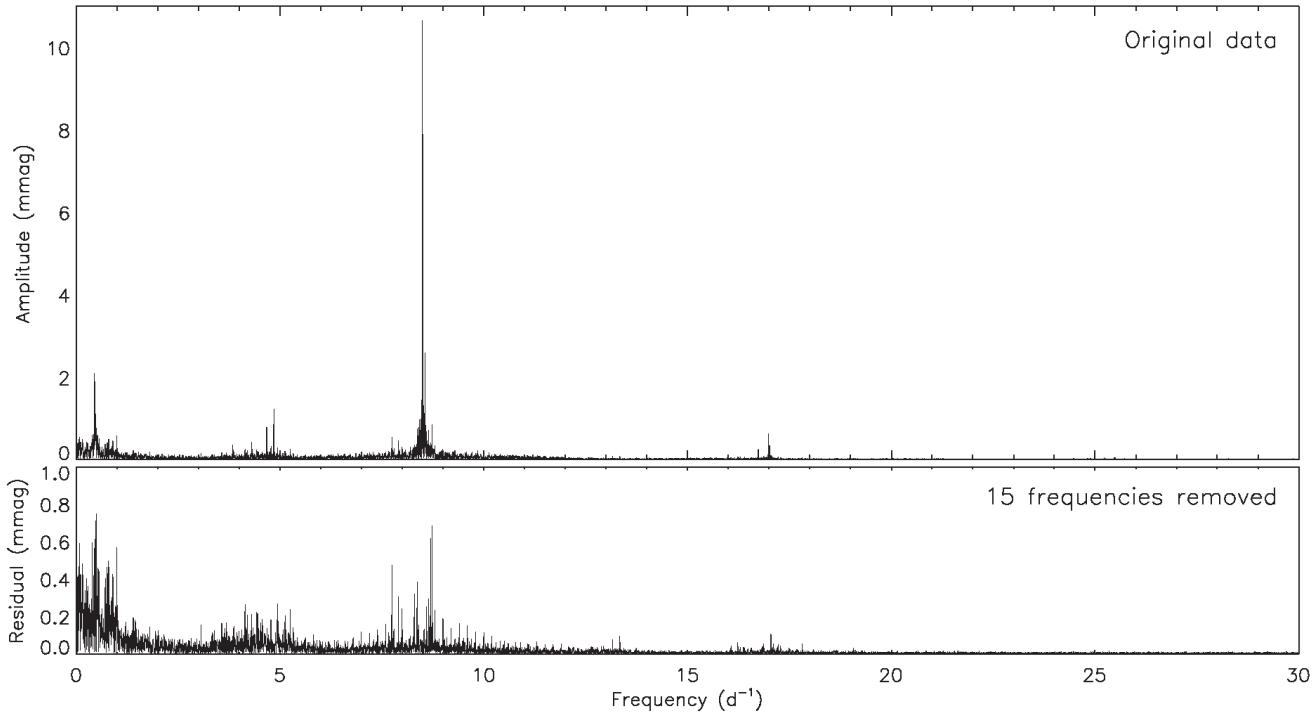

FIG. 3

Frequency spectrum of the *TESS* light-curve of GK Dra. Top: frequency spectrum of the data after subtraction of the binary model. Bottom: frequency spectrum after subtraction of the binary model and the 15 frequencies measured in this work.

of frequencies around 3·8–4·8 d^{-1} (f_4 to f_7), 8·5 d^{-1} (f_8 and f_9), 16·7–17·0 d^{-1} (f_{10} to f_{12}) and 25·2–25·5 d^{-1} (f_{13} to f_{15}), of the δ Scuti type. The frequency spectum of the residuals in Fig. 3 shows excess power in several frequency intervals, suggesting there are additional pulsations below our S/N criterion which might be measurable using additional data.

We conclude that the GK Dra system probably contains at least one hybrid δ Sct / γ Dor star — the caveat here is that we know which is the pulsating star for only one of the frequencies so it is conceivable than one component produces the g-modes and the other the p-modes. Either way, this is an interesting system. None of the frequencies identified here correspond to multiples of the orbital frequency, so we find no evidence for tidally induced or perturbed pulsations. GK Dra has been observed for two sets of 13 consecutive sectors by *TESS*, with a third one scheduled, so is a good candidate for searching for amplitude modulation in a δ Scuti star of known mass and radius[50].

We also calculated frequency spectra of the 600-s-cadence data from sectors 47 to 60, expecting that the additional data would yield a cleaner spectrum with a lower noise floor. However, the resulting spectra all contained combs of aliases of the strongest frequencies separated by multiples of the orbital frequency; note that these were not seen in the 200-s data. This problem occurred using both the residuals of the JKTEBOP best fit, the original data, the original data with the eclipses removed, and the original data with the points during eclipse set to zero magnitude. GK Dra will benefit from a more detailed analysis in future, preferably including data from *TESS* sectors 73 to 83 that are scheduled for observation beginning in 2023 December.

Chromospheric emission

We obtained a spectrum of the Ca II *H* and *K* lines of GK Dra, alongside other objects in this series[51,52], in order to probe for chromospheric emission lines indicative of magnetic activity. The current target was selected based on its G0 spectral type listed in *Simbad*, which is much later than it should be (see above). GK Dra is thus not a promising target for chromospheric emission, but the spectrum only cost about 8 minutes of observing time.

The spectrum was obtained on the night of 2022/06/07 in excellent weather conditions, using the *Isaac Newton Telescope* (*INT*) and *Intermediate Dispersion Spectrograph* (*IDS*), the 235-mm camera, the H2400B grating, the EEV10 CCD, a 1-arcsec slit, and an exposure time of 180 s. It covers 373–438 nm at a reciprocal dispersion of 0·023 nm px^{-1} and a signal-to-noise ratio of approximately 150, and was taken at an orbital phase of 0·19. Data reduction was performed using a pipeline currently being written by the author[53].

The spectrum is shown in Fig. 4, which also includes a synthetic spectrum for a $T_{\rm eff}$ of 7000 K and a log g of 4·0 from the BT-Settl model atmospheres[54,55]. The Ca *H* and *K* line centres have a higher flux than those in the synthetic spectrum, but this can be attributed to the binarity (RV difference at the time of observation) and rotational velocities of the stars. Thus there is no clear evidence for chromospheric emission (as expected).

Physical properties of GK Dra

Based on the analysis presented above and published results for the system, we have determined the physical properties of GK Dra. We adopted the values of $r_{\rm A}$, $r_{\rm B}$, P, and i from the 600-s-cadence data in Table II, doubling the error bars as described above. For the velocity amplitudes of the system we used the

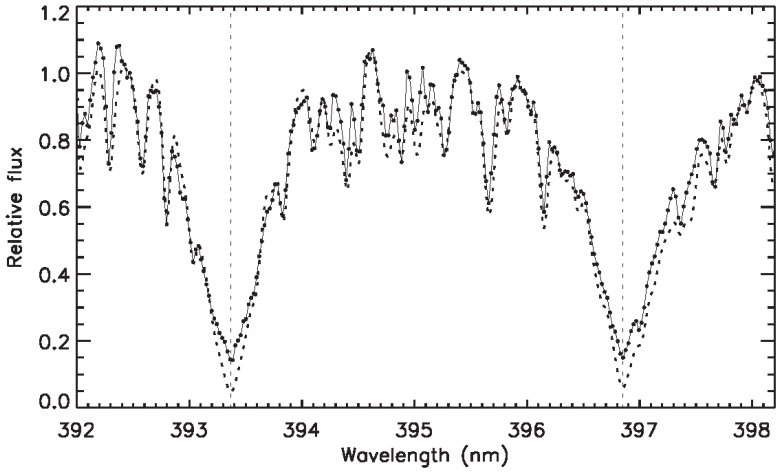

FIG. 4

Observed spectrum of GK Dra around the Ca II *H* and *K* lines (solid line with points) compared to a synthetic spectrum for a star with $T_{\rm eff}$ = 7000 K, log g = 4·0, and solar metallicity from the BT-Settl model atmospheres (dashed line) smoothed to the observed spectral resolution. The *H*- and *K*- line central wavelengths are shown with dotted lines. Both spectra have been normalized and shifted to zero velocity.

results from GB03 directly as these authors carefully accounted for the effects of pulsations in the RVs: we adopted $K_{\rm A}$ = 81·14 ± 0·60 km s^{-1} and $K_{\rm B}$ = 64·97 ± 0·13 km s^{-1} after interchanging the numbers to account for the differing definitions of which is the primary star. The $T_{\rm eff}$ values were taken directly from ZW03 — these correspond to spectral types of F1 and F2 on the calibration given by Pecaut & Mamajek[57] and are thus much earlier than the G0 given in the *Henry Draper Catalogue*[21].

The physical properties were then calculated using the JKTABSDIM code[58] and entered into Table IV. The radii are measured to 0·7% (star A) and 1·0% (star B)

TABLE IV

Physical properties of GK Dra defined using the nominal solar units given by IAU 2015 Resolution B3 (ref. 56). The $T_{\rm eff}$ values are from ZW03.

Parameter	*Star A*	*Star B*
Mass ratio $M_{\rm B}/M_{\rm A}$	1·249 ± 0·010	
Semi-major axis of relative orbit ($R_\odot^{\rm N}$)	28·72 ± 0·12	
Mass ($M_\odot^{\rm N}$)	1·421 ± 0·012	1·775 ± 0·028
Radius ($R_\odot^{\rm N}$)	1·634 ± 0·011	2·859 ± 0·028
Surface gravity (log[cgs])	4·1642 ± 0·0044	3·7749 ± 0·0083
Density ($\rho_\odot$)	0·3257 ± 0·0050	0·0760 ± 0·0020
Synchronous rotational velocity (km s^{-1})	8·29 ± 0·05	14·50 ± 0·14
Effective temperature (K)	7100 ± 70	6878 ± 57
Luminosity log($L/L_\odot^{\rm N}$)	0·786 ± 0·018	1·217 ± 0·017
$M_{\rm bol}$ (mag)	2·774 ± 0·045	1·698 ± 0·042
Distance (pc)	306·9 ± 4·8	

precision, limited by the results of the light-curve analysis, and the masses to 1·0% (star A) and 1·6% (star B) precision, limited by the effect of pulsations on the RVs of star B. The radius measurement of star A is very different from that of ZW03 ($R_A = 2{\cdot}431 \pm 0{\cdot}042\ R_\odot$) whereas for star B the values are consistent (ZW03 obtained $R_B = 2{\cdot}830 \pm 0{\cdot}054\ R_\odot$). This can be attributed to the extraordinary improvement in the quality of the *TESS* light-curve *versus* that previously available, and suggests the older error bars were significantly underestimated.

To test our results we determined the distance to GK Dra using the surface-brightness calibrations of Kervella *et al.*[59] for comparison with the *Gaia* parallax. We adopted the apparent magnitudes given in Table I, but with the 2MASS JHK_s values converted to the Johnson system[60]. Setting an interstellar reddening of zero gives consistent distances in the five passbands. The most precise is that in K_s, $306{\cdot}9 \pm 4{\cdot}8$ pc, which we adopt as our final value. This compares favourably with the *Gaia* DR3[33,20] parallax distance of $303{\cdot}5 \pm 1{\cdot}2$ pc, suggesting that the radii and $T_{\rm eff}$ values in Table IV are reliable. As further evidence, the ratio of the $T_{\rm eff}$ values found by ZW03 is in perfect agreement with the surface-brightness ratio we found from the light-curve (Table II).

Comparison with theoretical models

GK Dra B shows significant evolution and is now cooler than GK Dra A despite its greater mass. We thus decided to compare the measured properties of GK Dra to the predictions of the PARSEC 1·2S theoretical stellar-evolutionary models[61,62]. The best fit was found in the mass–radius and mass–$T_{\rm eff}$ diagrams[63] for an age of 1400 ± 50 Myr and a fractional metal abundance of $Z = 0{\cdot}014$. The age measurement is very sensitive to the properties of star B, and once the age is set the $T_{\rm eff}$ of star A is the primary determinant of the best Z value. The quoted age and Z provide an excellent match to the properties of star B, but star A is approximately 2σ larger and hotter than predicted. A better agreement could be obtained by interpolation between the $Z = 0{\cdot}010$ and $= 0{\cdot}014$ models, but this is outside the scope of the current work.

We illustrate these results in a Hertzsprung–Russell diagram in Fig. 5. In this plot are a zero-age main sequence, evolutionary tracks for masses 1·2, 1·4, 1·6, 1·8, and $2{\cdot}0\ M_\odot$, and an isochrone for age 1400 Myr, all for a metal abundance of $Z = 0{\cdot}014$. The isochrone provides a good but not perfect match to the properties of GK Dra.

Summary and conclusions

The eclipsing nature of GK Dra was discovered from *Hipparcos* photometry, and subsequent ground-based photometry and spectroscopy allowed the discovery of pulsations in the more massive star and approximate physical properties of this star and its companion. We have revisited GK Dra and used the extensive photometry available from the *TESS* mission to improve our understanding of the system. We find that the eclipses are total, and determine the masses and radii of the stars to high precision. These match the predictions of theoretical models for an age of 1·4 Gyr and a slightly subsolar metallicity.

The *TESS* data allow the detection and measurement of 15 significant pulsation frequencies, three of which are have low frequencies in the region of $0{\cdot}5\ {\rm d}^{-1}$ so arise from the γ Dor phenomenon, and the remaining 12 of which form four groups of higher frequencies consistent with δ Scuti pulsations. By far the strongest frequency is at $f_8 = 8{\cdot}49\ {\rm d}^{-1}$, and this one has been detected

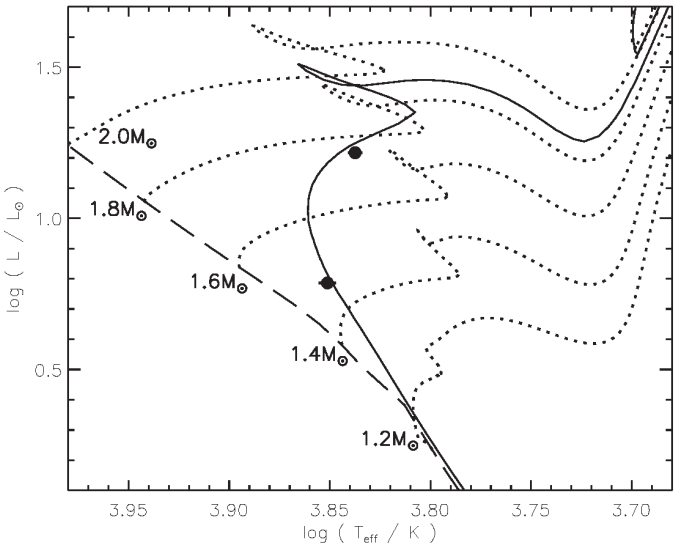

FIG. 5

Hertzsprung–Russell diagram for the components of GK Dra (filled circles with error bars) and the predictions of the PARSEC 1·2S models for selected masses (dotted lines with masses labelled) and the zero-age main sequence (dashed line), for a metal abundance of $Z = 0{\cdot}014$. The 1·4-Gyr isochrone is shown with a solid line.

spectroscopically in the more evolved star B. GK Dra almost certainly contains one or two hybrid γ Dor/δ Sct stars, and more extensive data are expected to reveal further pulsation frequencies.

The measured properties of GK Dra are now sufficiently precise and accurate to be included in the *Detached Eclipsing Binary Catalogue* (*DEBCat*[⋆], ref. 64). *TESS* is scheduled to observe GK Dra between 2023 December and 2024 September. A detailed asteroseismic analysis of these data, once available, is recommended.

Acknowledgements

We thank the anonymous referee for a positive report. This paper includes data collected by the *TESS* mission and obtained from the MAST data archive at the Space Telescope Science Institute (STScI). Funding for the *TESS* mission is provided by the NASA's Science Mission Directorate. STScI is operated by the Association of Universities for Research in Astronomy, Inc., under NASA contract NAS 5–26555. This work has made use of data from the European Space Agency (ESA) mission *Gaia*[†], processed by the *Gaia* Data Processing and Analysis Consortium (DPAC[‡]). Funding for the DPAC has been provided by national institutions, in particular the institutions participating in the *Gaia* Multilateral Agreement. The following resources were used in the course of this work: the NASA Astrophysics Data System; the *Simbad* database operated at CDS, Strasbourg, France; and the arχiv scientific paper preprint service operated by Cornell University.

⋆https://www.astro.keele.ac.uk/jkt/debcat/

†https://www.cosmos.esa.int/gaia

‡https://www.cosmos.esa.int/web/gaia/dpac/consortium

References

(1) J. Higl & A. Weiss, *A&A*, **608**, A62, 2017.
(2) A. Claret & G. Torres, *ApJ*, **859**, 100, 2018.
(3) A. Tkachenko *et al.*, *A&A*, **637**, A60, 2020.
(4) C. Aerts, J. Christensen-Dalsgaard & D. W. Kurtz, *Asteroseismology* (Springer), 2010.
(5) C. Aerts *et al.*, *Science*, **300**, 1926, 2003.
(6) M. Briquet *et al.*, *MNRAS*, **381**, 1482, 2007.
(7) A. García Hernández *et al.*, *A&A*, **559**, A63, 2013.
(8) T. R. Bedding *et al.*, *Nature*, **581**, 147, 2020.
(9) J. Southworth, *Universe*, **7**, 369, 2021.
(10) P. Gaulme & J. A. Guzik, *A&A*, **630**, A106, 2019.
(11) X. Chen *et al.*, *ApJS*, **263**, 34, 2022.
(12) F. Kahraman Aliçavuş *et al.*, *MNRAS*, **524**, 619, 2023.
(13) M. Breger, in *Delta Scuti and Related Stars* (M. Breger & M. Montgomery, ed.), 2000, *Astronomical Society of the Pacific Conference Series*, vol. 210, pp. 3–42.
(14) A. Grigahcène *et al.*, *ApJ*, **713**, L192, 2010.
(15) J. Debosscher *et al.*, *A&A*, **556**, A56, 2013.
(16) J. Southworth & T. Van Reeth, *MNRAS*, **515**, 2755, 2022.
(17) G. W. Henry, F. C. Fekel & S. M. Henry, *AJ*, **133**, 1421, 2007.
(18) L. A. Balona, J. Daszyńska-Daszkiewicz & A. A. Pamyatnykh, *MNRAS*, **452**, 3073, 2015.
(19) J. Southworth, *The Observatory*, **140**, 247, 2020.
(20) Gaia Collaboration, *A&A*, **649**, A1, 2021.
(21) A. J. Cannon & E. C. Pickering, *Annals of Harvard College Observatory*, **96**, 1, 1921.
(22) K. G. Stassun *et al.*, *AJ*, **158**, 138, 2019.
(23) E. Høg *et al.*, *A&A*, **355**, L27, 2000.
(24) R. M. Cutri *et al.*, 2MASS *All Sky Catalogue of Point Sources* (The IRSA 2MASS All-Sky Point Source Catalogue, NASA/IPAC Infrared Science Archive, Caltech, US), 2003.
(25) ESA (ed.), *The Hipparcos and Tycho catalogues. Astrometric and photometric star catalogues derived from the ESA Hipparcos space astrometry mission*, *ESA Special Publication*, vol. 1200, 1997.
(26) E. V. Kazarovets *et al.*, *IBVS*, **4659**, 1, 1999.
(27) S. Dallaporta *et al.*, *IBVS*, **5312**, 1, 2002.
(28) A. Liakos & P. Niarchos, *MNRAS*, **465**, 1181, 2017.
(29) F. Kahraman Aliçavuş *et al.*, *MNRAS*, **470**, 915, 2017.
(30) R. F. Griffin & H. M. J. Boffin, *The Observatory*, **123**, 203, 2003.
(31) P. F. L. Maxted *et al.*, *A&A*, **578**, A25, 2015.
(32) T. Zwitter *et al.*, *A&A*, **404**, 333, 2003.
(33) Gaia Collaboration, *A&A*, **595**, A1, 2016.
(34) G. R. Ricker *et al.*, *Journal of Astronomical Telescopes, Instruments, and Systems*, **1**, 014003, 2015.
(35) Lightkurve Collaboration, '(Lightkurve: Kepler and *TESS* time series analysis in Python)', Astrophysics Source Code Library, 2018.
(36) J. M. Jenkins *et al.*, in *Proc. SPIE*, 2016, *Society of Photo-Optical Instrumentation Engineers (SPIE) Conference Series*, vol. 9913, p. 99133E.
(37) J. Southworth, P. F. L. Maxted & B. Smalley, *MNRAS*, **351**, 1277, 2004.
(38) J. Southworth, *A&A*, **557**, A119, 2013.
(39) D. Hestroffer, *A&A*, **327**, 199, 1997.
(40) J. Southworth, *The Observatory*, **143**, 71, 2023.
(41) A. Claret & J. Southworth, *A&A*, **664**, A128, 2022.
(42) A. Claret & J. Southworth, *A&A*, **674**, A63, 2023.
(43) J. Southworth, *MNRAS*, **417**, 2166, 2011.
(44) J. Southworth, *MNRAS*, **386**, 1644, 2008.
(45) J. Southworth, *The Observatory*, **141**, 234, 2021.
(46) J. Southworth, *The Observatory*, **143**, 254, 2023.
(47) P. Lenz & M. Breger, *Communications in Asteroseismology*, **146**, 53, 2005.
(48) M. Breger *et al.*, *A&A*, **271**, 482, 1993.
(49) R. Kuschnig *et al.*, *A&A*, **328**, 544, 1997.
(50) D. M. Bowman *et al.*, *MNRAS*, **460**, 1970, 2016.
(51) J. Southworth, *The Observatory*, **142**, 267, 2022.
(52) J. Southworth, *The Observatory*, **143**, 19, 2023.
(53) J. Southworth *et al.*, *MNRAS*, **497**, 4416, 2020.
(54) F. Allard *et al.*, *ApJ*, **556**, 357, 2001.
(55) F. Allard, D. Homeier & B. Freytag, *Phil. Trans. Series A*, **370**, 2765, 2012.
(56) A. Prša *et al.*, *AJ*, **152**, 41, 2016.
(57) M. J. Pecaut & E. E. Mamajek, *ApJS*, **208**, 9, 2013.
(58) J. Southworth, P. F. L. Maxted & B. Smalley, *A&A*, **429**, 645, 2005.
(59) P. Kervella *et al.*, *A&A*, **426**, 297, 2004.

(60) J. M. Carpenter, *AJ*, **121**, 2851, 2001.
(61) A. Bressan *et al.*, *MNRAS*, **427**, 127, 2012.
(62) Y. Chen *et al.*, *MNRAS*, **444**, 2525, 2014.
(63) J. Southworth & J. V. Clausen, *A&A*, **461**, 1077, 2007.
(64) J. Southworth, in *Living Together: Planets, Host Stars and Binaries* (S. M. Rucinski, G. Torres & M. Zejda, eds.), 2015, *Astronomical Society of the Pacific Conference Series*, vol. 496, p. 321.

REVIEWS

Supermassive Black Holes, by Andrew King (Cambridge University Press), 2023. Pp. 308, 25 × 17·5 cm. Price £54·99/$69·99 (hardbound; ISBN 978 1 108 48805 1).

Recently, supermassive black holes have garnered significant attention, captivating both the public and scientists alike. The no-hair theorem states that any black hole can be completely described by its mass, angular momentum, and charge; nevertheless, a multitude of intricate phenomena emerge from these systems. The past decade has seen ground-breaking advances, such as the direct detection of gravitational waves from merging stellar-mass and intermediate-mass black holes as well as the imaging of black-hole shadows by the *Event Horizon Telescope*.

Looking towards the future, black-hole science holds immense promise, especially with electromagnetic facilities such as *JWST* pushing detections of supermassive black holes to higher redshifts, and next-generation gravitational-wave detectors, such as *LISA* and *IPTA*, targeting the supermassive black-hole regime. Notably, strong observational hints at a gravitational-wave background formed from the cosmic population of supermassive binary black holes detected by *IPTA* have further intensified the excitement.

Amidst this backdrop, Andrew King's book, *Supermassive Black Holes*, proves to be a timely and relevant textbook in the current research landscape. It masterfully weaves together the theories of General Relativity and fluid dynamics with the rich phenomenology of active galactic nuclei (AGN) and the co-evolution of supermassive black holes and their host galaxies. The book comprises eight chapters, where the initial four lay the essential groundwork for the cutting-edge research topics explored in the latter four.

In the first chapter, the author outlines crucial theoretical concepts and observational characteristics of supermassive black holes. Moving on, the second chapter serves as a summary of the salient features of General Relativity concerning black holes, catering to both those familiar with GR and newcomers. The third chapter focusses on astrophysical gasses, encompassing fluid dynamics in various relevant regimes, including incompressible flows, shocks, plasma theory, and magnetohydrodynamics. The author establishes connections to different astrophysical scenarios, discussing the applicability of standard approximations while cautioning against quasi-Newtonian treatments. Chapter 4 delves into accretion-disc theory, starting with Newtonian orbits